International Journal of Heat and Mass Transfer 51 (2008) 5279–5287

Contents lists available at ScienceDirect

International Journal of Heat and Mass Transfer

journal homepage: www.elsevier.com/locate/ijhmt

Computation of turbulent free convection in left and right tilted porous enclosures using a macroscopic k–ε model

Edimilson J. Braga, Marcelo J.S. de Lemos *

Departamento de Energia – IEME, Instituto Tecnológico de Aeronáutica – ITA, 12228-900 São José dos Campos, SP, Brazil

ARTICLE INFO

Article history:
Received 23 July 2007
Received in revised form 14 March 2008
Available online 28 May 2008

Keywords:
Porous media
Heat transfer
Natural convection

ABSTRACT

Comparisons of computations for turbulent natural convection within clockwise and counter-clockwise inclined cavities, filled with a fluid saturated porous medium, are presented. The finite volume method in a generalized coordinate system is applied. Oblique walls are maintained at constant but different temperatures, whereas horizontal surfaces are kept insulated. Flow and heat transfer characteristics are investigated for Rayleigh number up to 10^4 and inclination angles up to 45°, in both directions of rotation. Turbulent is handled using a macroscopic two-equation model with a wall function. In this work, the turbulence model is first switched off and the laminar branch of the solution is obtained. Subsequently, the turbulence model is included and the solution merges to the laminar branch for a reducing value of Ra_m. Present computations are compared with published results and the influence of the inclination angle on Ra_{cr} is analyzed, for both the left and right rotating directions. For Ra_m greater than around 10^4, both laminar and turbulent flow solutions deviate, possibly indicating that a critical value for Ra_m was reached. Both left and right rotation of the hot wall reduce Nu, but rotating the hot wall on the counter-clockwise direction decreases Nu at a faster rate than when bending the cavity to the right.

1. Introduction

The study of buoyancy driven flows in both clear and porous domains has several applications in many fields of science, technology and environment. In addition, if the Reynolds number based on the mean porous diameter is higher than 300, there might be sufficient "room" in the void space for turbulence to be established. In fact, modeling of important environmental and engineering flows using a macroscopic view, resorting to a porous medium model, is found in the study of atmospheric boundary layer over dense rain forests, in the underground spread of pollutants, in the analysis of heat exchangers, in cooling devices for electronic equipment, in grain storage, in nuclear reactor safety and in may other applications. In all cases above, instead of looking at a detailed distribution of the flow field within the void phase, both fluid and solid components are treated by a unique set of equations via appropriate volume-averaging tools. As such, the existence of turbulence in the fluid phase, analyzed with macroscopic equations and based on a porous medium model, gives rise to the study of Turbulence in Porous Media.

There are many studies concerning laminar flow in porous media in the available literature. The monographs of Nield and Bejan [1] and Ingham and Pop [2] fully documented the problem of a laminar flow in a porous medium. The case of natural convection in a rectangular cavity heated on a side and cooled at the opposing side is an important problem in thermal convection in porous media and the works of Walker and Homsy [3], Bejan [4], Prasad and Kulacki [5], Beckermann et al. [6], Gross et al. [7], Manole and Lage [8] and Moya et al. [9] have contributed with some important results to this problem. The work of Baytas and Pop [10] concerned a numerical study of the steady free convection flow in rectangular and oblique cavities filled with homogeneous porous media using a non-linear axis transformation. The Darcy momentum and energy equations are solved numerically using the (ADI) method. Turbulence, however, has never been the main subject of previous studies.

Modeling of macroscopic transport for incompressible flows in porous media has been based on the volume-average methodology for either heat [11] or mass transfer [12–14]. Accordingly, if time fluctuations of the flow properties are also considered, in addition to spatial deviations, there are two possible methodologies to follow in order to obtain turbulent macroscopic equations: (a) application of time average operator followed by volume-averaging [15–18] or (b) use of volume-averaging before time averaging is applied [19–21]. However, both sets of macroscopic mass transport equations are equivalent when examined under the recently established double decomposition concept [22–25].

This methodology, initially developed for the flow variables, has been extended to heat transfer in porous media where both time

* Corresponding author. Tel.: +55 12 3947 5860.
E-mail address: delemos@mec.ita.br (M.J.S. de Lemos).

0017-9310/$ - see front matter © 2008 Elsevier Ltd. All rights reserved.
doi:10.1016/j.ijheatmasstransfer.2008.03.016

Nomenclature

c_F	Forchheimer coefficient
$c's$	non-dimensional turbulence model constants
c_p	constant pressure specific heat
$\mathbf{D}$	$\mathbf{D}=[\nabla\mathbf{u}+(\nabla\mathbf{u})^T]/2$, Deformation rate tensor
Da	Darcy number, $Da = K/L^2$
D_p	particle diameter
$\mathbf{g}$	Gravity acceleration vector
G_k	buoyancy production rate of turbulent kinetic energy
G^i	generation rate of $\langle k\rangle^i$ due to the action of the porous matrix
G^i_β	generation rate of $\langle k\rangle^i$ due to the buoyant effects
h	heat transfer coefficient
$\mathbf{I}$	unit tensor
K	$K=\frac{D_p^2\phi^3}{144(1-\phi)^2}$, permeability
k	$k=\overline{\mathbf{u}'\cdot\mathbf{u}'}/2$ Turbulent kinetic energy per mass unit
k_f	fluid thermal conductivity
k_s	solid thermal conductivity
k_{eff}	effective thermal conductivity
$\mathbf{K}_{disp}$	conductivity tensor due to the dispersion
$\mathbf{K}_{disp,t}$	conductivity tensor due to the turbulent dispersion
$\mathbf{K}_t$	conductivity tensor due to the turbulent heat flux
$\mathbf{K}_{tor}$	conductivity tensor due to the tortuosity
L	square width
$\mathbf{n}$	unit vector normal to the A_i
Nu	average Nusselt number, $Nu=\frac{1}{H}\int_0^H Nu_y\,dy;\ Nu_y=\frac{hH}{k_{eff}}=\left(\frac{\partial\langle T\rangle^v}{\partial x}\right)_{x=0}\frac{H}{T_H-T_C}$
P_k	Shear production rate of turbulent kinetic energy
P^i	Production rate of $\langle k\rangle^i$ due to gradients of $\bar{\mathbf{u}}_D$
Pr	Prandtl number
Ra_f	$Ra_f=\frac{g\beta L^3\Delta T}{\nu_f\alpha_f}$, fluid Rayleigh number
Ra_m	$Ra_m=Ra_f\cdot Da=\frac{g\beta_\phi L\Delta TK}{\nu_f\alpha_{eff}}$, Darcy–Rayleigh number
Ra_{cr}	critical Rayleigh number
T	temperature
$\mathbf{u}$	microscopic velocity
$\mathbf{u}_D$	Darcy or superficial velocity (volume average of $\mathbf{u}$)

Greek symbols

α	thermal diffusivity
β	thermal expansion coefficient
θ	inclination angle
ΔV	representative elementary volume
ΔV_f	fluid volume inside ΔV
ε	$\varepsilon=\mu\overline{\nabla\mathbf{u}':(\nabla\mathbf{u}')^T}/\rho$, dissipation rate of k
μ	dynamic viscosity
μ_{t_ϕ}	Macroscopic turbulent viscosity
ν	kinematic viscosity
ρ	density
$\sigma's$	non-dimensional constants
ϕ	$\phi=\Delta V_f/\Delta V$, porosity

Special characters

φ	general variable
$\bar{\varphi}$	time average
φ'	time fluctuation
$\langle\varphi\rangle^i$	intrinsic average
$\langle\varphi\rangle^v$	volume average
${}^i\varphi$	spatial deviation
$\lvert\varphi\rvert$	absolute value (Abs)
$\boldsymbol{\varphi}$	general vector variable
$(\,)_{s,f}$	solid/fluid
$(\,)^T$	transpose
$(\,)_{eff}$	effective value, $\phi\varphi_f+(1-\phi)\varphi_s$
$(\,)_{H,C}$	hot/cold
$(\,)_\phi$	macroscopic value

fluctuations and spatial deviations were considered for velocity and temperature [26,27]. Studies on the treatment of interface condition [28,29] and a general classification of all proposed models for turbulent flow and heat transfer in porous media [30] have also been published. Extension of the double decomposition theory for treating turbulent natural convection [31–34], mass transfer [35], non-equilibrium heat transfer [36,37] and double diffusion [38] in saturated rigid porous media has also been recently documented.

Motivated by the foregoing works, this paper presents results for both laminar and turbulent flows in oblique cavities, inclined towards both directions, which is totally filled with a porous material and are heated from the left and cooled from the opposing side. The other two walls are kept insulated. The turbulence model here adopted is the macroscopic k–ε with the wall function. To the best of the authors' knowledge, no comparison on the behavior of the cavity Nusselt number, considering both inclination directions, has been previously published. The contribution herein presents such comparison, including the cases when the flow is in turbulent regime.

2. The problem considered

The problem considered is showed schematically in Fig. 1 and refers to an oblique cavities with width $L = 1$ m completely filled with porous medium. The cavity is isothermally heated from the left, T_H, and cooled from the opposing side, T_C. The other two walls are insulated. The porous medium is considered to be rigid and satured by an incompressible fluid. The Ra_m is the dimensionless parameter used for porous media and it is defined as, $Ra_m = Ra_f Da$, with $\alpha_{eff} = k_{eff}/(\rho c_p)_f$ and the particle diameter is given by $D_p=\sqrt{\frac{144K(1-\phi)^2}{\phi^3}}$.

3. Governing equations

The equations used herein are derived in details in the works of Pedras and de Lemos [23], de Lemos and Rocamora [27] and de Lemos and Braga [32]. Basically, for porous media analysis, a macroscopic form of the governing equations is obtained by taking the volumetric average of the entire equation set. In that development, the porous medium was considered to be rigid and saturated by an incompressible fluid.

The macroscopic continuity equation is given by,

$$\nabla\cdot\bar{\mathbf{u}}_D=0 \tag{1}$$

The Dupuit–Forchheimer relationship, $\bar{\mathbf{u}}_D=\phi\langle\bar{\mathbf{u}}\rangle^i$, has been used and $\langle\bar{\mathbf{u}}\rangle^i$ identifies the intrinsic (liquid) average of the local velocity vector $\bar{\mathbf{u}}$. The macroscopic time-mean Navier–Stokes (NS) equation for an incompressible fluid with constant properties is given as

$$\rho\left[\frac{\partial\bar{\mathbf{u}}_D}{\partial t}+\nabla\cdot\left(\frac{\bar{\mathbf{u}}_D\bar{\mathbf{u}}_D}{\phi}\right)\right]=-\nabla(\phi\langle\bar{p}\rangle^i)+\mu\nabla^2\bar{\mathbf{u}}_D+\nabla\cdot(-\rho\phi\langle\overline{\mathbf{u}'\mathbf{u}'}\rangle^i)-\rho\beta_\phi\mathbf{g}\phi(\langle\bar{T}\rangle^i-T_{ref})-\left[\frac{\mu\phi}{K}\bar{\mathbf{u}}_D+\frac{c_F\phi\rho|\bar{\mathbf{u}}_D|\bar{\mathbf{u}}_D}{\sqrt{K}}\right] \tag{2}$$

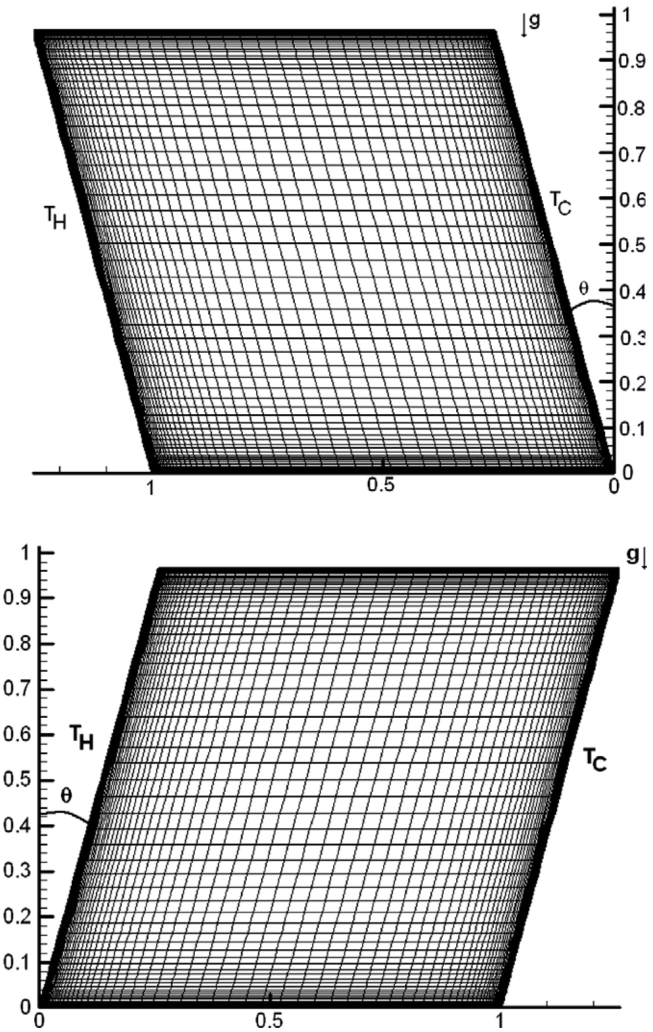

Fig. 1. Geometry and grid under consideration: (a) counter-clockwise direction and (b) clockwise direction.

When treating turbulence with statistical tools, the correlation $-\rho\overline{\mathbf{u}'\mathbf{u}'}$ appears after application of the time average operator to the local instantaneous NS equation. Applying further the volume-average procedure to this correlation results in the term $-\rho\phi\langle\overline{\mathbf{u}'\mathbf{u}'}\rangle^i$. This term is here called the Macroscopic Reynolds Stress Tensor (MRST). Further, a model for the MRST in analogy with the Boussinesq concept for clear fluid can be written as

$$-\rho\phi\langle\overline{\mathbf{u}'\mathbf{u}'}\rangle^i = \mu_{t_\phi}2\langle\overline{\mathbf{D}}\rangle^{\mathbf{v}} - \frac{2}{3}\phi\rho\langle k\rangle^i\mathbf{I} \tag{3}$$

where

$$\langle\overline{\mathbf{D}}\rangle^v = \frac{1}{2}[\nabla(\phi\langle\bar{\mathbf{u}}\rangle^i) + [\nabla(\phi\langle\bar{\mathbf{u}}\rangle^i)]^{\mathrm{T}}] \tag{4}$$

is the macroscopic deformation rate tensor, $\langle k\rangle^i$ is the intrinsic average for turbulent kinetic energy, k and μ_{t_ϕ} is the macroscopic turbulent viscosity. The macroscopic turbulent viscosity, μ_{t_ϕ}, is modeled similarly to the case of clear fluid flow and a proposal for it was presented in [23] as

$$\mu_{t_\phi} = \rho C_\mu\frac{\langle k\rangle^{i^2}}{\langle\varepsilon\rangle^i} \tag{5}$$

In a similar way, applying both time and volumetric average to the microscopic energy equation, for either the fluid or the porous matrix, two equations arise. Assuming further the Local Thermal Equilibrium Hypothesis, which considers $\langle\overline{T_f}\rangle^i = \langle\overline{T_s}\rangle^i = \langle\overline{T}\rangle^i$, and adding up these two equations, one has,

$$(\rho c_p)_f\nabla\cdot(\phi\langle\overline{\mathbf{u}T_f}\rangle^i) = (\rho c_p)_f\nabla\cdot\left\{\phi(\langle\bar{\mathbf{u}}\rangle^i\langle\overline{T_f}\rangle^i + \overline{\langle\mathbf{u}'\rangle^i\langle T_f'\rangle^i} + \langle{}^i\bar{\mathbf{u}}{}^i\overline{T_f}\rangle^i + \langle{}^i\overline{\mathbf{u}'{}^iT_f'}\rangle^i)\right\} \tag{6}$$

A modeled form of (6) has been given in detail in the work of de Lemos and Rocamora [27] as

$$\{(\rho c_p)_f\phi + (\rho c_p)_s(1-\phi)\}\frac{\partial\langle\overline{T}\rangle^i}{\partial t} + (\rho c_p)_f\nabla\cdot(\bar{\mathbf{u}}_D\langle\overline{T}\rangle^i) = \nabla\cdot\{\mathbf{K}_{\mathrm{eff}}\cdot\nabla\langle\overline{T}\rangle^i\} \tag{7}$$

where $\mathbf{K}_{\mathrm{eff}}$ given by

$$\mathbf{K}_{\mathrm{eff}} = [\phi k_f + (1-\phi)k_s]\mathbf{I} + \mathbf{K}_{\mathrm{tor}} + \mathbf{K}_t + \mathbf{K}_{\mathrm{disp}} + \mathbf{K}_{\mathrm{disp,t}} \tag{8}$$

is the effective conductivity tensor. In order to be able to apply (7), it is necessary to determine the conductivity tensors in (8), i.e. $\mathbf{K}_{\mathrm{tor}}$, $\mathbf{K}_t$, $\mathbf{K}_{\mathrm{disp}}$ and $\mathbf{K}_{\mathrm{disp,t}}$. Following [17], this can be accomplished for the tortuosity and thermal dispersion conductivity tensors, $\mathbf{K}_{\mathrm{tor}}$ and $\mathbf{K}_{\mathrm{disp}}$, by making use of a unit cell subjected to periodic boundary conditions for the flow and a linear temperature gradient imposed over the domain. The conductivity tensors are then obtained directly from the microscopic results for the unit cell (see [17] for details on the expressions here used).

The turbulent heat flux and turbulent thermal dispersion terms, $\mathbf{K}_t$ and $\mathbf{K}_{\mathrm{disp,t}}$, which cannot be determined from such a microscopic calculation, are modeled here through the Eddy diffusivity concept, similarly to Nakayama and Kuwahara [18]. It should be noticed that these terms arise only if the flow is turbulent, whereas the tortuosity and the thermal dispersion terms exist for both laminar and turbulent flow regimes.

Starting out from the time averaged energy equation coupled with the microscopic modeling for the 'turbulent thermal stress tensor' through the Eddy diffusivity concept, one can write, after volume averaging,

$$-(\rho c_p)_f\langle\overline{\mathbf{u}'T_f'}\rangle^i = (\rho c_p)_f\frac{\nu_{t_\phi}}{\sigma_T}\nabla\langle\overline{T_f}\rangle^i \tag{9}$$

where the symbol ν_{t_ϕ} expresses the macroscopic eddy viscosity, $\mu_{t_\phi} = \rho_f\nu_{t_\phi}$, given by (5) and σ_T is a constant. According to (9), the macroscopic heat flux due to turbulence is taken as the sum of the turbulent heat flux and the turbulent thermal dispersion found by de Lemos and Rocamora [27]. In view of the arguments given above, the turbulent heat flux and turbulent thermal dispersion components of the conductivity tensor, $\mathbf{K}_t$ and $\mathbf{K}_{\mathrm{disp,t}}$, respectively, are expressed as

$$\mathbf{K}_t + \mathbf{K}_{\mathrm{disp,t}} = \phi(\rho c_p)_f\frac{\nu_{t_\phi}}{\sigma_T}\mathbf{I} \tag{10}$$

In the all equations shown above, when $\phi = 1$ and the permeability K tends to infinite, the domain is considered as a clear medium. For any other value of ϕ, the domain is treated as a porous medium.

4. Turbulence model

Transport equations for $\langle k\rangle^i = \langle\overline{\mathbf{u}'\cdot\mathbf{u}'}\rangle^i/2$ and $\langle\varepsilon\rangle^i = \mu\langle\overline{\nabla\mathbf{u}':(\nabla\mathbf{u}')^{\mathrm{T}}}\rangle^i/\rho$ in their so-called High Reynolds number form are fully documented in [23] making use of the double decomposition concept [22], and extended in [31,32] to incorporate the buoyant effects. Basically, for porous media analysis, a macroscopic form of the governing equations is here obtained by taking the volumetric average of the time averaged equations set. It is important to emphasize that the parameter Reynolds number, while not considered as a basic parameter in natural convection flows, is here recalled with the sole purpose of characterizing the turbulent regime and the corresponding wall treatment used.

On the other hand, in both works of Lee and Howell [19] and Antohe and Lage [20] was developed a macroscopic equation for turbulent kinetic energy from the macroscopic momentum equation. According to Pedras and de Lemos [23], the kinetic energy used in [19,20] differs from $\langle k\rangle^i$ and is given by $k_m = \overline{\langle \mathbf{u}'\rangle^i \cdot \langle \mathbf{u}'\rangle^i}/2$. Pedras and de Lemos [23] have shown that the relationship between these two quantities as being

$$\begin{aligned}\langle k\rangle^i &= \overline{\langle \mathbf{u}'\cdot\mathbf{u}'\rangle^i}/2 = \overline{\langle \mathbf{u}'\rangle^i \cdot \langle \mathbf{u}'\rangle^i}/2 + \overline{\langle {}^i\mathbf{u}'\cdot {}^i\mathbf{u}'\rangle}/2 \\ &= k_m + \overline{\langle {}^i\mathbf{u}'\cdot {}^i\mathbf{u}'\rangle}/2 \qquad (11)\end{aligned}$$

The last term on the right-hand side of (14) is the extra turbulent kinetic energy and for that reason, models based on km do not account for all of the turbulent kinetic energy associated with the flow.

Therefore, the macroscopic turbulent transport equations presented in [23] and extended in [31] are given by

$$\rho\left[\frac{\partial}{\partial t}(\phi\langle k\rangle^i) + \nabla\cdot(\bar{\mathbf{u}}_D\langle k\rangle^i)\right] = \nabla\cdot\left[\left(\mu+\frac{\mu_{t_\phi}}{\sigma_k}\right)\nabla(\phi\langle k\rangle^i)\right] + P^i + G^i + G^i_\beta - \rho\phi\langle\varepsilon\rangle^i \qquad (12)$$

$$\rho\left[\frac{\partial}{\partial t}\left(\phi\langle\varepsilon\rangle^i\right) + \nabla\cdot(\bar{\mathbf{u}}_D\langle\varepsilon\rangle^i)\right] = \nabla\cdot\left[\left(\mu+\frac{\mu_{t_\phi}}{\sigma_\varepsilon}\right)\nabla(\phi\langle\varepsilon\rangle^i)\right] + c_1 P^i\frac{\langle\varepsilon\rangle^i}{\langle k\rangle^i} + c_2\frac{\langle\varepsilon\rangle^i}{\langle k\rangle^i}G^i + c_1 c_3 G^i_\beta\frac{\langle\varepsilon\rangle^i}{\langle k\rangle^i} - c_2\rho\phi\frac{\langle\varepsilon\rangle^{i2}}{\langle k\rangle^i} \qquad (13)$$

where c_1, c_2, c_3 and c_k are constants, $P^i = (-\rho\langle\overline{\mathbf{u}'\mathbf{u}'}\rangle^i : \nabla\bar{\mathbf{u}}_D)$ is the production rate of $\langle k\rangle^i$ due to gradients of $\bar{\mathbf{u}}_D$, $G^i = c_k\rho\frac{\phi\langle k\rangle^i|\bar{\mathbf{u}}_D|}{\sqrt{K}}$ is the generation rate of the intrinsic average of k due to the action of the porous matrix and $G^i_\beta = \phi\frac{\mu_{t_\phi}}{\sigma_t}\beta_\phi\mathbf{g}\cdot\nabla\langle\overline{T}\rangle^i$ is the generation rate of $\langle k\rangle^i$ due to the buoyant effects.

The constants of the standard k–ε turbulence model in Eqs. (5), (12) and (13), according to Launder and Spalding [39] for a clear medium ($\phi = 1$ and $K\to\infty$), are given by

$$c_\mu = 0.09,\quad c_1 = 1.44,\quad c_2 = 1.92,\quad c_3 = 1.0,\quad \sigma_k = 1.0,\quad \sigma_\varepsilon = 1.3,\quad \sigma_T = 0.9 \qquad (14)$$

For a porous medium, these constants can present different values of those presented above. However, as a first approximation, they were taken as equal to those in (14), as suggested in the work of Lee and Howell [19].

5. Numerical method and solution procedure

The numerical method employed for discretizing the governing equations is the control-volume approach with a generalized grid. A hybrid scheme, Upwind Differencing Scheme (UDS) and Central Differencing Scheme (CDS), is used for interpolating the convective fluxes. The well-established SIMPLE algorithm [40] is followed for handling the pressure–velocity coupling. Individual algebraic equation sets were solved by the SIP procedure of Stone [41]. The present results were performed with $\phi = 0.8$, $Da = 10^{-7}$ and $K_{disp} = 0$. The Prandtl number and the conductivity ratio between the solid and fluid phases are assumed to be unity. It was used an 80×80 stretched grid. Concentration of nodal points to walls reduces eventual errors due to numerical diffusion which, in turn, are further annihilated due to the hybrid scheme here adopted.

6. Results and discussion

Problems of natural convection concerning cavities of different shapes arise from the need of developing passive techniques to enhance the heat transfer process across enclosures. As such, one of these passive techniques is the reshaping of the bounded region and the study of different sizes of cavities. Thus, either in cavities of 1 m side, as the one here computed, or in enclosures of a few millimeters high, detailed studies contribute to the design of passive heat transfer devices. In fact, the investigation herein is also of great importance in regard to miniaturization of electronic devices, which are severely constrained by space and weight. In the work herein two types of oblique cavities are investigated, namely with clockwise and counter-clockwise inclination.

It is also important to emphasize that the main objective of this work is not to detect the transition mechanism, from laminar regime to fully turbulent flow, which involves modeling of complex physical processes and hydrodynamic instabilities. Here the aim is to establish a Ra_{cr} where below it laminarization of the turbulent flow occurs. For clear flows, when Ra_f is varied, the literature often refers to laminar and turbulent "branches" of solutions as Ra_f passes a critical value. When a turbulence model is included, the turbulent solution can deviates from the laminar branch for $Ra_f > Ra_{cr}$ and follows its turbulent branch. Below a critical Ra_f number, the standard k–ε model gives a turbulent viscosity, which is close to zero everywhere. This reduction of turbulent transfer can be interpreted as an indication of the laminarization phenomenon. However, above this critical value, the turbulent viscosity suddenly increases and a turbulent solution is obtained.

In the work of Braga and de Lemos [32], a Ra_{cr} for a porous square cavity was found. This value was about $Ra_{cr} = 10^4$ and was not sensible to small variations in the Darcy number, Da or due to the consideration of dispersion (K_{disp}) mechanism. This work studies the influence of a clockwise and a counter-clockwise inclination angle on the Ra_{cr} in an oblique cavity. Thus, as done in [32,34] the turbulence model is first switched off and the laminar branch of the solution is found when increasing the Rayleigh number, Ra_m. Subsequently, the turbulence model is included so that the solution merges to the laminar branch for $Ra_m < Ra_{cr}$. Here, it is important to emphasize that, similarly to Braga and de Lemos [32], the turbulent branch of the solution was obtained by reducing the value of Ra to a point where no differences were detected when using the two models. Reproduction of this "laminarization" path,

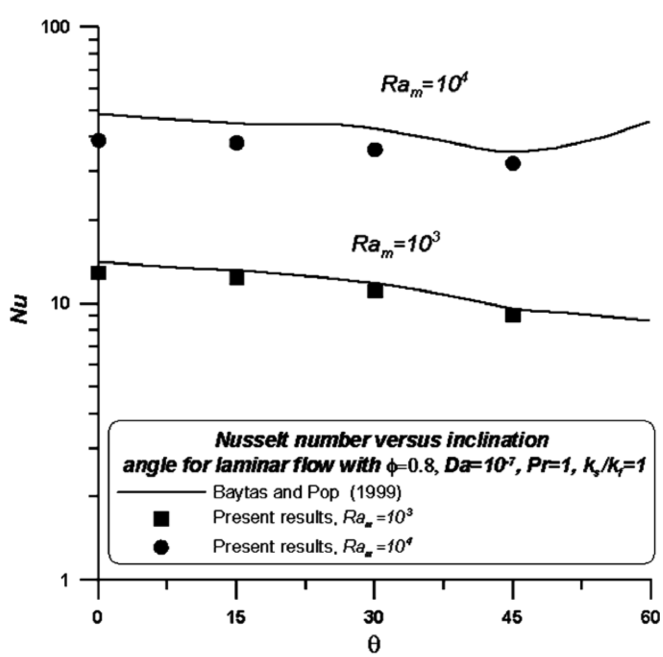

Fig. 2. Average Nusselt numbers for tilted cavities.

already mentioned above, was in fact the main motivation for the development of the k–ε model more than three decades ago [42].

Fig. 2 shows the average Nusselt number for laminar flow for a clockwise inclination with $Ra_m = 10^3$ and 10^4 for $Da = 10^{-7}$, $\phi = 0.8$, $k_s/k_f = 1$, $Pr = 1$ for several angles. The shows that, the higher the inclination angle, the lower is the average Nusselt number at the hot wall. A possible explanation for such behavior is reduction of the available area for the recirculatory flow as the inclination angle increases.

Further, Fig. 3 shows streamlines and isotherms for the turbulent model solution for a counter-clockwise inclination cavity of $Ra_m = 10^5$. The streamlines shown in Fig. 3 indicate a small dependence with the angle variation. For the range of inclination angles analyzed, the higher the inclination angle, the lower the overall values of recirculation intensity. On the other hand, the isotherms are stratified for the three angles analyzed and the inclination angle seems not to affect the isotherms significantly and the main mechanism of heat transport is by convection mechanism.

Fig. 4 shows the streamlines and isotherms for the turbulent model solution for a clockwise inclination cavity of $Ra_m = 10^5$. The streamlines show a small dependence with the angle variation. For the range of inclination angles analyzed, the higher the inclination angle, the lower the overall values of recirculation intensity. This behavior is probably due to the positive inclination that acts like an obstacle for the ascendant buoyant flow near to the heated wall and due to the reduction of the space inside the enclosure. The isotherms are also stratified for the three angles analyzed and the inclination angle do not play an important hole in the isotherms, so that, the main mechanism of heat transport is by convection mechanism.

Table 1 shows the average Nusselt number at the hot wall for the two types of regime, namely laminar and turbulent, for various,

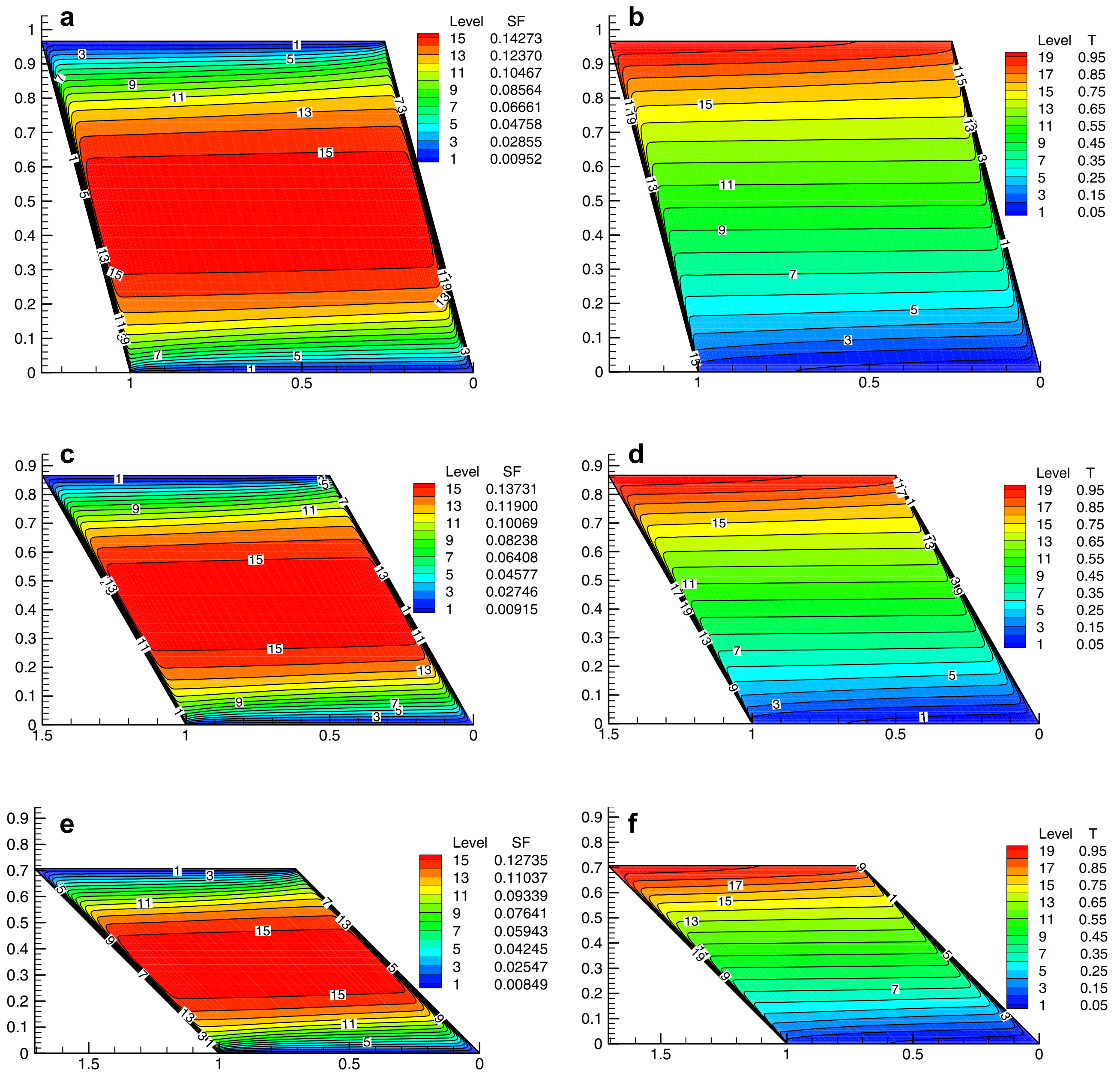

Fig. 3. Streamlines (left) and isotherms (right) for turbulent model solution for a cavity with a counter-clockwise inclination with $Ra_m = 10^5$, $\phi = 0.8$, $Da = 10^{-7}$, $k_s/k_f = 1$, $Pr = 1$; (a,b) $\theta = 15°$, (c,d) $\theta = 30°$, (e,f) $\theta = 45°$.

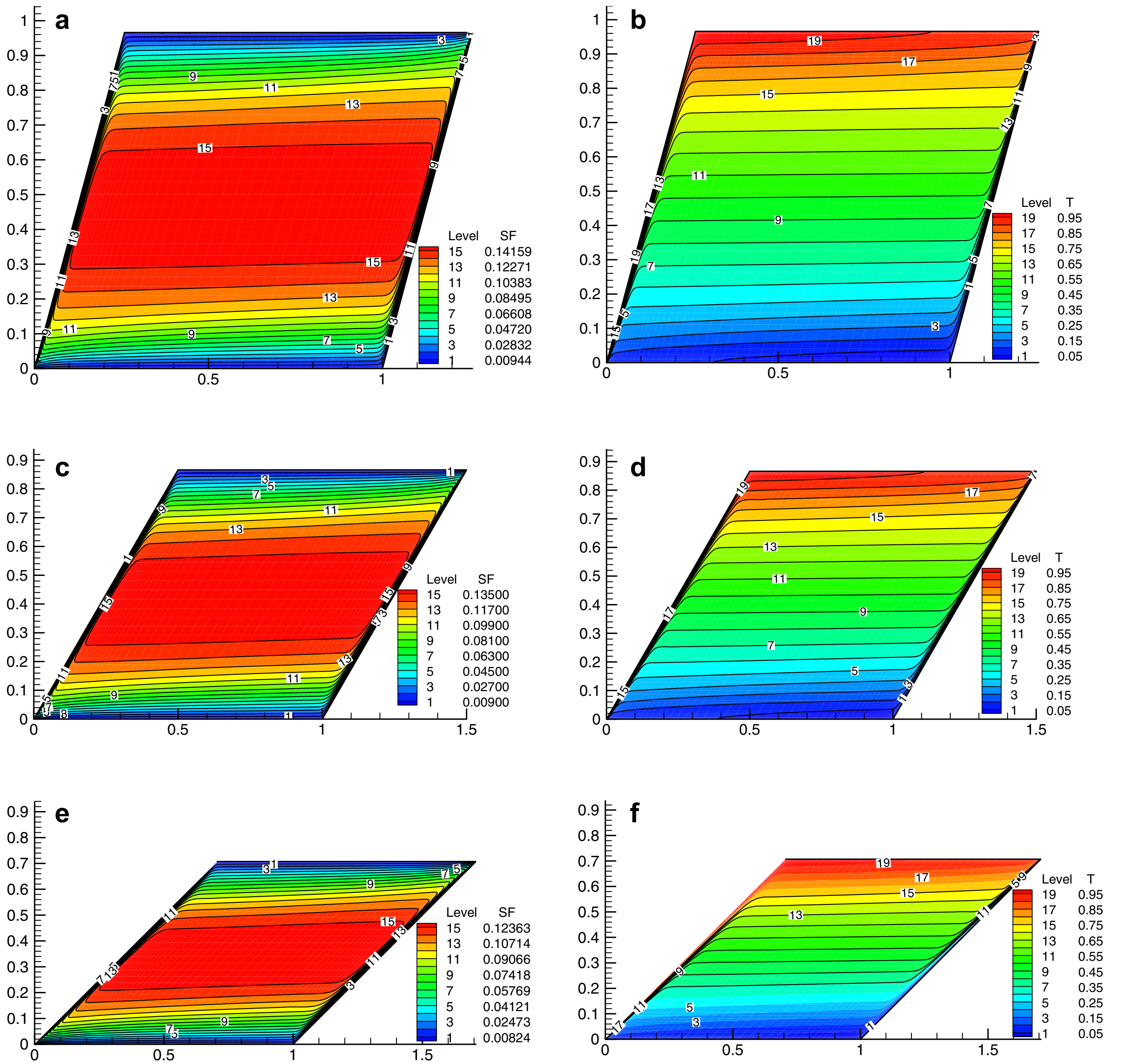

Fig. 4. Streamlines (left) and isotherms (right) for turbulent model solution for a cavity with a clockwise inclination with $Ra_m = 10^5$, $\phi = 0.8$, $Da = 10^{-7}$, $k_s/k_f = 1$, $Pr = 1$; (a,b) $\theta = 15°$, (c,d) $\theta = 30°$, (e,f) $\theta = 45°$.

and θ. Inspecting Table 1 one can see that the turbulent solution departs from the laminar one for Ra_m greater than about 10^4. Consequently, the calculations herein suggest that a critical value for Rayleigh–Darcy number, Ra_m, is also of the order of 10^4 and from that value on simulations considering a turbulence model gives a higher value of Nu than their laminar counterpart. It was observed that the overall values of Nu for higher inclination angles are smaller than those for lower inclinations. Ultimately, it seems that the inclination angle does not affect the point where the deviation occurs for the range of angles analyzed.

Table 2 shows the average Nusselt number at the hot wall for the two types of regime, namely laminar and turbulent, for various Ra_m and θ. The table shows that the turbulent solution departs from the laminar one also for Ra_m greater than about 10^4. Consequently, the calculations herein suggest that a critical value for Rayleigh–Darcy number, Ra_m, is also of the order of 10^4 and from that value on simulations considering a turbulence model gives a

Table 1
Comparison between laminar and turbulent model solutions for the average Nusselt number at the hot wall for a cavity with counter-clockwise inclination angle $\theta = 0°$, 15°, 30°, 45°, respectively, and Ra_m ranging from 10^3 to 10^5 with $Da = 10^{-7}$, $\phi = 0.8$, $k_s/k_f = 1$, $Pr = 1$

Model solution/Ra_m	10^3	10^4	10^5
$\theta = 0°$			
Laminar model	12.9310	38.9716	88.4639
$k-\varepsilon$ model	13.0326	40.6142	101.6477
$\theta = 15°$			
Laminar model	12.8900	38.4983	87.4852
k–ε model	12.9937	40.1084	100.4768
$\theta = 30°$			
Laminar model	12.2365	36.7182	84.2690
k–ε model	12.3272	38.1392	96.2246
$\theta = 45°$			
Laminar model	10.9776	33.4860	78.4577
k–ε model	11.0464	34.5895	88.4691

Table 2
Comparison between laminar and turbulent model solutions for the average Nusselt number at the hot wall for a cavity with clockwise inclination angle $\theta = 0°$, 15°, 30°, 45°, respectively, and Ra_m ranging from 10^3 to 10^5 with $Da = 10^{-7}$, $\phi = 0.8$, $k_s/k_f = 1$, $Pr = 1$

Model solution/Ra_m	10^3	10^4	10^5
$\theta = 0°$			
Laminar model	12.9310	38.9716	88.4639
k–ε model	13.0326	40.6142	101.6477
$\theta = 15°$			
Laminar model	12.3622	38.1886	87.3490
k–ε model	12.4473	39.6990	99.8880
$\theta = 30°$			
Laminar model	11.1117	36.0252	83.9821
k–ε model	11.1717	37.2610	95.0257
$\theta = 45°$			
Laminar model	9.0899	32.1553	77.8913
k–ε model	9.1411	32.9969	86.5605

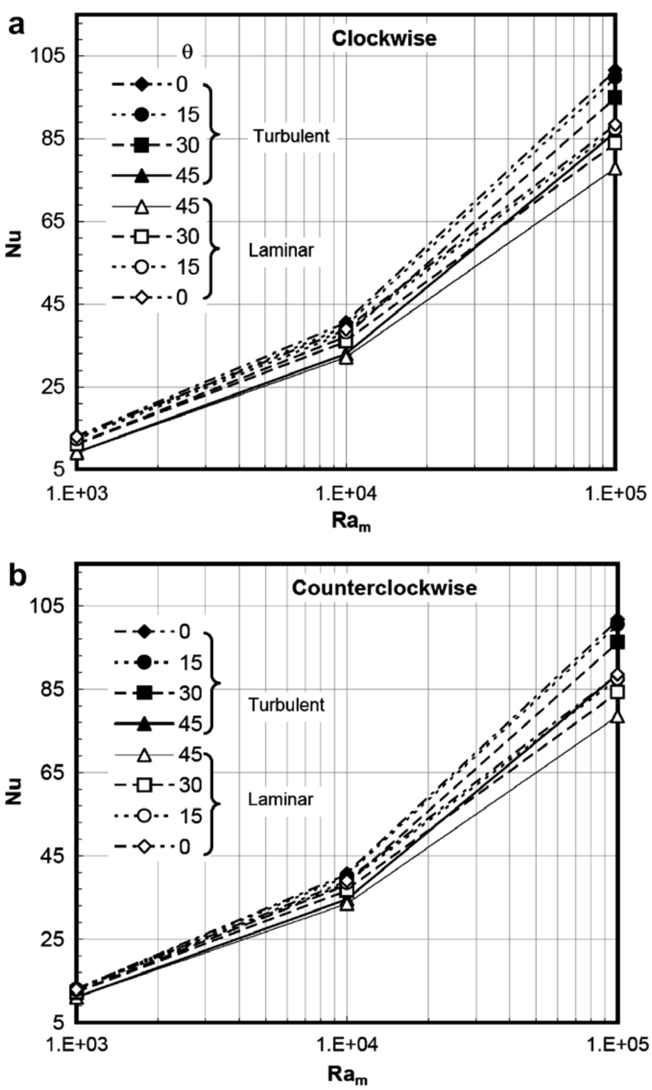

Fig. 5. Average Nusselt number as a function of model and Ra_m: (a) clockwise inclination and (b) counter-clockwise inclination.

higher value of Nu than their laminar counterpart. It was observed that the overall values of Nu for higher inclination angles are smaller than those for lower inclinations. Also, it seems that the inclination angle does not affect the point where the bifurcation occurs

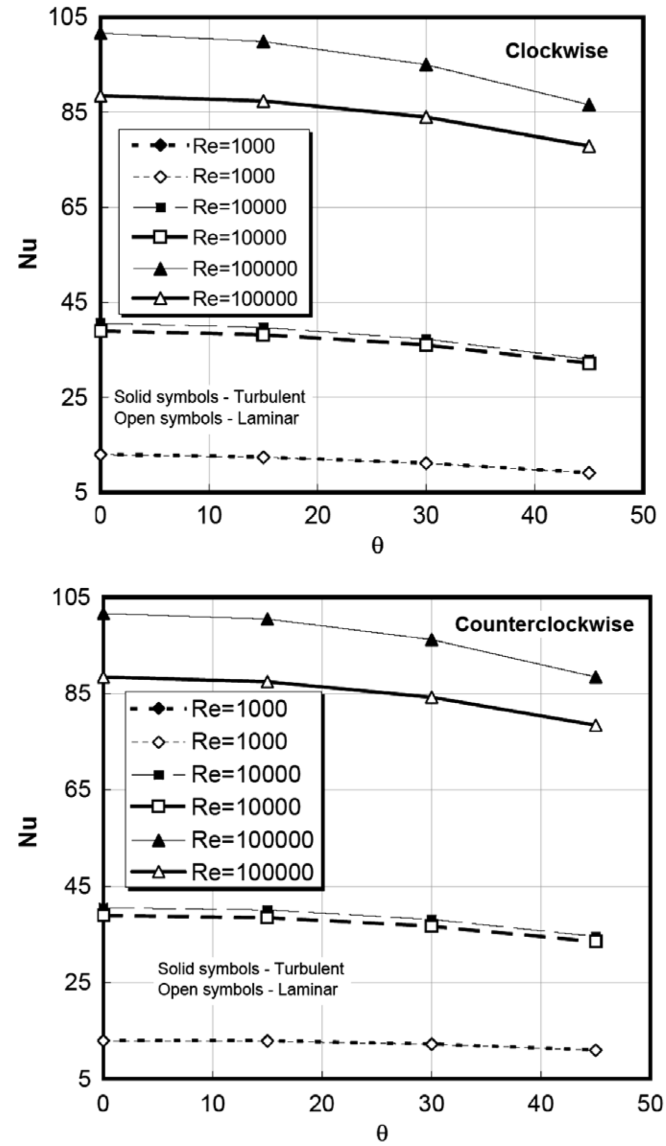

Fig. 6. Average Nusselt number as a function of model and θ: (a) clockwise inclination and (b) counter-clockwise inclination.

for the range of angles analyzed. From the table results it is observed that the overall Nusselt values for cavities with counterclockwise inclination are slightly higher than those obtained for the cavities with clockwise inclination angles. Results in Tables 1 and 2 can be better visualized next.

Fig. 5 plots average Nusselt numbers as a function of Ra_m for both angle orientations, which where illustrated by Fig. 1. For either angular direction, Nu computed with a turbulence model is greater for higher values of Ra_m, indicating that a departure from the laminar branch of the solution has probably started. The effect of angle θ on Nu is further shown in Fig. 6, also for both cavity inclinations. In both clockwise and counter-clockwise directions, a slight reduction on Nu is observed, for either the laminar solution or when the k–ε model is applied. Such reduction when varying θ is greater for larger Rayleigh number, indicating that for low speed flows the overall transport currents between walls is less sensitive on θ. Reduction of Nu, using both models for either direction, seems to reflect a reduction in the overall cavity area, which apparently impairs heat transfer by reducing convective currents within the cavity.

In order to access which inclination direction has the most influence on Nu, a relative Nusselt defined as Nu_{cw}/Nu_{ccw}, where

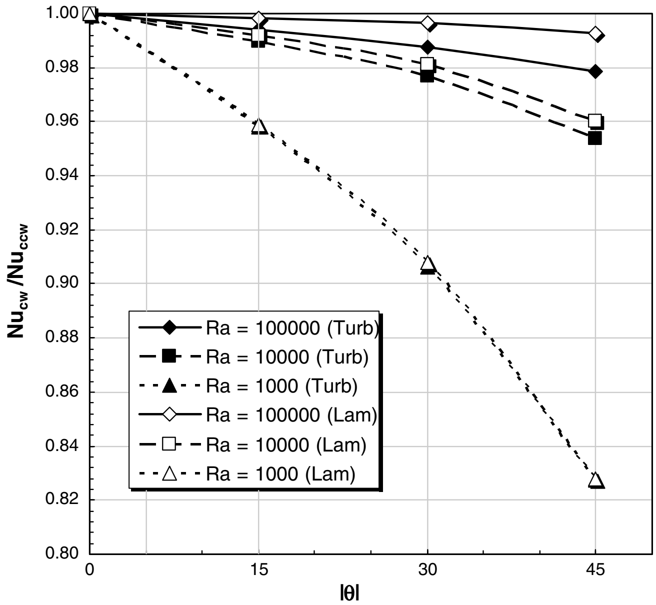

Fig. 7. Relative *Nu* damping as a function of cavity inclination: solid symbols – turbulence model, open symbols – laminar model.

the subscripts refers to the rotation direction, is defined. Fig. 7 finally shows results for such relative *Nu* as a function of the angle modulus, $|\theta|$. One can observe that clockwise cavity rotations will always reduce heat transfer in a more efficient manner, regardless of the Rayleigh number applied (Nu_{cw} always less than Nu_{ccw}). This could be explained due to the fact that, although both Nu_{cw} and Nu_{ccw} decrease with cavity rotation, due to the effective area reduction mentioned above, a counter-clockwise rotation brings the hot wall to an overall "lower" level, whereas the clockwise rotation tends towards bringing the configuration closer to a cavity heated from above. As such, although a rotation to the left decreases convective currents due to reduction of flow area (Fig. 6b), the tendency towards an unconditionally unstable heated-from-below cavity case does that at a lower rate than in the case of a rotation to the right (Fig. 6a). Also observed from Fig. 7 is that the lower the Ra_m, the greater the reduction on *Nu* when varying θ on both rotating directions. Also, as expected, for low Ra_m flows no detectable difference exists when *Nu* is computed with both mathematical models. Finally observed in Fig. 7 is that for higher values of $|\theta|$ and for large Ra_m the two solutions present the most discrepancy when calculating *Nu*.

7. Conclusions

Computations for laminar and turbulent flows with the macroscopic k–ε model with a wall function for natural convection in oblique cavities totally filled with porous material were performed. The calculations herein suggest that a critical value for Ra_m is of the order of 10^4. Additional conclusions of this work are:

(a) In either rotating direction, the average Nusselt numbers for horizontal heat transfer is decreased for a porous square cavity. This behavior is probably due to the overall cross-sectional area reduction, acting as an obstacle for the ascendant buoyant flow near to the heated wall, as well as due to the reduction of the effective cavity height with rotation.
(b) The inclination angle does not affect the point where both the laminar and turbulent solutions deviate from each other, at least for the range of angles here analyzed.
(c) The overall Nusselt values for oblique cavities with counter-clockwise inclination are slightly higher than those obtained for oblique cavities with the same clockwise inclination. This effect might be associated with the fact that turning the hot wall to the left reduces *Nu* but, at the same time, brings the hot wall to a lower overall height, tending towards the unconditionally unstable cases of cavities heated from below. The opposite trend is observed for right rotations of the hot wall, leading to unconditionally stable heated-from-above cases, which, in turn, further damps convective currents within the cavity.

Ultimately, the study herein is expected to be useful to engineering design of systems such as packed electronics.

Acknowledgement

The authors are thankful to CNPq and FAPESP, Brazil, for their invaluable financial support during the course of this research.

References

[1] D.A. Nield, A. Bejan, Convection in Porous Media, Springer, New York, 1992.
[2] D.B. Ingham, I. Pop, Transport Phenomena in Porous Media, Elsevier, Amsterdam, 1998.
[3] K.L. Walker, G.M. Homsy, Convection in porous cavity, J. Fluid Mech. 87 (1978) 449–474.
[4] A. Bejan, On the boundary layer regime in a vertical enclosure filled with a porous medium, Lett. Heat Mass transfer 6 (1979) 93–102.
[5] V. Prasad, F.A. Kulacki, Convective heat transfer in a rectangular porous cavity-effect of aspect ratio on flow structure and heat transfer, J. Heat Transfer 106 (1984) 158–165.
[6] C. Beckermann, R. Viskanta, S. Ramadhyani, A numerical study of non-Darcian natural convection in a vertical enclosure filled with a porous medium, Numer. Heat Transfer 10 (1986) 557–570.
[7] R.J. Gross, M.R. Bear, C.E. Hickox, The Application of flux-corrected transport (FCT) to high rayleigh number natural convection in a porous medium, in: Proceedings of the 8th International Heat Transfer Conference, CA, 1986.
[8] D.M. Manole, J.L. Lage, Numerical benchmark results for natural convection in a porous medium cavity, HTD, Heat Mass Transfer Porous Media, ASME Conference 216 (1992) 55–60.
[9] S.L. Moya, E. Ramos, M. Sen, Numerical study of natural convection in a tilted rectangular porous material, Int. J. Heat Mass Transfer 30 (1987) 741–756.
[10] A.C. Baytas, I. Pop, Free convection in oblique enclosures filled with a porous medium, Int. J. Heat Mass Transfer 42 (1999) 1047–1057.
[11] C.T. Hsu, P. Cheng, Thermal dispersion in a porous medium, Int. J. Heat Mass Transfer 33 (1990) 1587–1597.
[12] J. Bear, Dynamics of Fluids in Porous Media, American Elsevier Publ. Co., New York, 1972.
[13] S. Whitaker, Equations of motion in porous media, Chem. Eng. Sci. 21 (1966) 291–300.
[14] S. Whitaker, Diffusion and dispersion in porous media, J. Amer. Inst. Chem. Eng. 13 (3) (1967) 420–427.
[15] T. Masuoka, Y. Takatsu, Turbulence model for flow through porous media, Int. J. Heat Mass Transfer 39 (13) (1996) 2803–2809.
[16] F. Kuwahara, A. Nakayama, H. Koyama, A numerical study of thermal dispersion in porous media, J. Heat Transfer 118 (1996) 756–761.
[17] F. Kuwahara, A. Nakayama, Numerical modeling of non-Darcy convective flow in a porous medium, in: Heat Transfer 1998, Proceedings of the 11th International Heat Transfer Conference, vol. 4, Taylor & Francis, Kyongyu, Korea, Washington, DC, 1998.
[18] A. Nakayama, F. Kuwahara, A macroscopic turbulence model for flow in a porous medium, J. Fluids Eng. 121 (1999) 427–433.
[19] K. Lee, J.R. Howell, Forced convective and radiative transfer within a highly porous layer exposed to a turbulent external flow field, Proceedings of the 1987 ASME-JSME Thermal Engineering Joint Conference, vol. 2, ASME, Honolulu, Hawaii, New York, NY, 1987.
[20] B.V. Antohe, J.L. Lage, A general two-equation macroscopic turbulence model for incompressible flow in porous media, Int. J. Heat Mass Transfer 40 (13) (1997) 3013–3024.
[21] D. Getachewa, W.J. Minkowycz, J.L. Lage, A modified form of the k–ε model for turbulent flow of a incompressible fluid in porous media, Int. J. Heat Mass Transfer 43 (2000) 2909–2915.
[22] M.H.J. Pedras, M.J.S. de Lemos, On the definition of turbulent kinetic energy for flow in porous media, Int. Commun. Heat Mass Transfer 27 (2) (2000) 211–220.
[23] M.H.J. Pedras, M.J.S. de Lemos, Macroscopic turbulence modeling for incompressible flow through undeformable porous media, Int. J. Heat Mass Transfer 44 (6) (2001) 1081–1093.

[24] M.H.J. Pedras, M.J.S. de Lemos, Simulation of turbulent flow in porous media using a spatially periodic array and a low-re two-equation closure, Numer. Heat Transfer A – Appl. 39 (1) (2001) 35–59.
[25] M.H.J. Pedras, M.J.S. de Lemos, On the mathematical description and simulation of turbulent flow in a porous medium formed by an array of elliptic rods, J. Fluids Eng. 123 (4) (2001) 941–947.
[26] F.D. Rocamora Jr., M.J.S. de Lemos, Analysis of convective heat transfer of turbulent flow in saturated porous media, Int. Commun. Heat Mass Transfer 27 (6) (2000) 825–834.
[27] M.J.S. de Lemos, F.D. Rocamora, Turbulent transport modeling for heated flow in rigid porous media, in: Proceedings of the Twelfth International Heat Transfer Conference, 2002, pp. 791–795.
[28] R.A. Silva, M.J.S. de Lemos, Numerical analysis of the shear stress jump for turbulent flow between in to flat plates, Int. J. Heat Mass Transfer, USA 46 (26) (2003) 5113–5121.
[29] R.A. Silva, M.J.S. de Lemos, Numerical analysis of the stress jump interface condition for laminar flow over a porous layer, Numer. Heat Transfer A – Appl., USA 43 (6) (2003) 603–617.
[30] M.J.S. de Lemos, M.H.J. Pedras, Recent mathematical models for turbulent flow for saturated rigid porous media, J. Fluids Eng. 123 (4) (2001) 935–940.
[31] M.J.S. de Lemos, E.J. Braga, Modeling of turbulent natural convection in saturated rigid porous media, Int. Commun. Heat Mass Transfer 30 (5) (2003) 615–624.
[32] E.J. Braga, M.J.S. de Lemos, Turbulent natural convection in a porous square cavity computed with a macroscopic k–ε model, Int. J. Heat Mass Transfer 47 (26) (2004) 5639–5650.
[33] E.J. Braga, M.J.S. de Lemos, Heat transfer in enclosures having a fixed amount of solid material simulated with heterogeneous and homogeneous models, Int. J. Heat Mass Transfer 48 (23–24) (2005) 4748–4765.
[34] E.J. Braga, M.J.S. de Lemos, Simulation of turbulent natural convection in a porous cylindrical annulus using a macroscopic two-equation model, Int. J. Heat Mass Transfer 49 (23–24) (2006) 4340–4351.
[35] M.J.S. de Lemos, M.S. Mesquita, Turbulent mass transport in saturated rigid porous media, Int. Commun. Heat Mass Transfer 30 (1) (2003) 105–113.
[36] M.B. Saito, M.J.S. de Lemos, Interfacial heat transfer coefficient for non-equilibrium convective transport in porous media, Int. Commun. Heat Mass Transfer 32 (5) (2005) 667–677.
[37] M.B. Saito, M.J.S. de Lemos, A correlation for interfacial heat transfer coefficient for turbulent flow over an array of square rods, J. Heat Transfer 128 (2006) 444–452.
[38] M.J.S. de Lemos, L.A. Tofaneli, Modeling of double-diffusive turbulent natural convection in porous media, Int. J. Heat Mass Transfer 47 (19–20) (2004) 4221–4231.
[39] B.E. Launder, D.B. Spalding, The numerical computation of turbulent flows, Comput. Methods Appl. Mech. Eng. 3 (1974) 269–289.
[40] S.V. Patankar, D.B. Spalding, A calculation procedure for heat, mass and momentum transfer in three dimensional parabolic flows, Int. J. Heat Mass Transfer 15 (1972) 1787.
[41] H.L. Stone, Iterative solution of implicit approximations of multi-dimensional partial differential equations, SIAM J. Numer. Anal. 5 (1968) 530–558.
[42] W.P. Jones, B.E. Launder, The prediction of laminarization with a two-equation model of turbulence, Int. J. Heat Mass Transfer 15 (1972) 301–314.